Deuterium atom loading of self-damaged tungsten at different sample temperatures

Anže Založnik[1], Sabina Markelj[1], Thomas Schwarz-Selinger[2], Klaus Schmid[2]

[1]Jozef Stefan institute, Jamova cesta 39, 1000 Ljubljana, Slovenia
[2]Max-Planck-Institut für Plasmaphysik, Boltzmannstrasse 2, D-85748 Garching, Germany

Abstract

The influence of surface parameters on hydrogen isotope atom absorption into tungsten material was studied. For this purpose a series of experiments was performed, exposing tungsten pre-damaged by tungsten ions, the so-called self-damaged W, to low energy deuterium atoms with the flux density of 4.2×10^{18} D/m^{2}s for 121 hours. Exposures were performed at four sample temperatures between 450 K and 600 K. Deuterium concentration was measured *in situ* and in real time during the exposure by nuclear reaction analysis. After the exposure, thermodesorption spectroscopy was performed on the samples. We have modeled the experimental data using a 1-D rate equation model and determined the detrapping energies and values of modeling parameters, which are describing deuterium atom adsorption on the surface of tungsten and migration of atoms from the surface to the bulk of the material. Assuming two adsorption site types, the determined surface adsorption energies are (0.68 ± 0.02) eV and (0.71 ± 0.02) eV and the activation energies for migration from the surface to the bulk are (1.41 ± 0.02) eV and (1.44 ± 0.02) eV, respectively. Modeling a low temperature plasma loading with the derived parameter set reveals that plasma loading experimental data could not be reproduced. We discuss possible reasons for the discrepancy between atom and plasma loading.

1 INTRODUCTION

Tungsten, as a chosen plasma-facing material for future fusion devices [1, 2], will be subjected to high fluxes of hydrogen isotope ions and neutral particles during the operation of a fusion device [3]. Retention of hydrogen isotopes in tungsten is of great importance, mainly because of the safety issues due to the radioactive nature of tritium [4]. Hydrogen retention in tungsten is very low, however the properties of the material change when heavily irradiated by high energy ions and neutrons. This introduces defects in the material, which act as strong binding sites or traps for hydrogen atoms, enhancing their retention in the material [5]. It was shown that retention increases for a couple of orders of magnitude when tungsten is damaged by neutrons, e.g. [6]. Neutron damaged samples are activated after neutron exposure, therefore high energy ion irradiation is often used as a surrogate for neutron irradiation, providing a fast and efficient way of simulating the displacement damage [7–10]. Very often MeV W ions are used for irradiation producing so-called self-damaged tungsten avoiding any chemical effects.

Due to the increased hydrogen isotope retention such self-damaged tungsten is also a good material to study the interaction of hydrogen isotopes with tungsten and effects of dislocation damage on e.g. hydrogen trapping [7] or isotope exchange [11]. Rate equation models can be applied to model the experimental results [12, 13]. The purpose of the present study is to

elaborate how low energy neutral hydrogen atoms can contribute to the retention in a fusion device as compared to ions with energies > 5 eV. Namely, in divertor region fluxes of low energy neutrals go up to 10^{24} m^{-2}s^{-1}, comparable to the ion fluxes [14].

High energy hydrogen ions can penetrate directly into the bulk of tungsten and the penetration depth depends on their kinetic energy [15]. The incoming low energy atoms, however, are limited to surface processes where they can adsorb on the surface of the material. From the surface they can recombine and leave the material or they can diffuse deeper in the bulk. There is a potential barrier for migration from the surface to the bulk of the material, responsible for low diffusion rate of H atoms into the bulk of W. To migrate to the subsurface an adsorbed atom needs to overcome the activation energy $E_{ch} + E_{bulk}$, where E_{ch} is the chemisorption energy on the surface of W and E_{bulk} is the potential barrier, defined as the sum of the heat of solution Q_s and the diffusion energy barrier E_{diff}. The rate of migration into the bulk is temperature dependent and the probability is increased at higher temperatures.

In order to study the rate of migration of low energy deuterium atoms into the bulk of tungsten, we have exposed self-ion damaged tungsten to low energy deuterium atoms (0.28 eV) at different sample temperatures from 450 K to 600 K. We have measured D concentration *in situ* during the D atom exposure by nuclear reaction analysis (NRA) at different exposure times. Additionally, thermodesorption spectroscopy (TDS) was performed on the samples *ex situ* after the loading and final D depth profile measurement. The experimental results of these two complementary techniques were modeled with a rate equation model. This enabled us to obtain information about surface adsorption sites and the activation energy for surface to bulk migration in W.

2 MODEL

To simulate of our experimental results we have used a 1-D rate equation model [12], called TESSIM. This model was developed for the simulation of deuterium ion implantation, diffusion and trapping in the bulk of tungsten [12]. Equations

$$\begin{aligned} \frac{\partial c^{sol}(x,t)}{\partial t} &= D(T(t))\frac{\partial^2 c^{sol}(x,t)}{\partial x^2} + S(x,t) - \sum_{i=1}^{N^{trap}} \frac{\partial c_i^{trap}(x,t)}{\partial t}, \\ \frac{\partial c_i^{trap}(x,t)}{\partial t} &= \frac{D(T(t))}{a_0^2 \beta} c^{sol}(x,t)\left(\eta_i(x,t) - c_i^{trap}(x,t)\right) - c_i^{trap}(x,t)\nu_i \mathrm{e}^{-E_i^{detrap}/k_B T(t)} \end{aligned} \tag{1}$$

are describing the concentration of solute hydrogen c^{sol}, which can diffuse between tetrahedral interstitial sites in W [16], and the concentration of trapped hydrogen c^{trap}, which is strongly bound in traps presented by crystal lattice defects of W. The top equation is the second Fick's law of diffusion of solute hydrogen with additional implantation term and trapping/detrapping term. Implantation in the bulk is described by $S(x,t) = \frac{\Gamma}{\rho_W}\xi(x)$, where Γ is the implantation flux and $\xi(x)$ is the implantation range distribution as a function of depth x with $x = 0$ being the surface. Trapping and detrapping processes are described by the bottom equation where the first term on the right-hand side describes trapping of solute hydrogen and the second term describes detrapping from the traps. Since different trap types

can exist, index $i = 1, \ldots, N^{trap}$ denotes individual trap types with the concentration of i-th trap type η_i, the attempt frequency to jump out of the trap ν_i and the detrapping energy E_i^{detrap}. For this study the attempt frequency is considered to be the same for all trap types, $\nu = 10^{13}$ s^{-1}. Hydrogen diffusion is described by a temperature dependent diffusion coefficient $D(T(t)) = D_0 \mathrm{e}^{-E_{diff}/k_B T(t)}$, where $D_0 = 4.1 \times 10^{-7}$ m^2/s [17] is the diffusion constant for H atoms and $E_{diff} = 0.39$ eV [17] is the diffusion energy barrier. The diffusion constant for D atoms is by a factor of $\sqrt{2}$ lower, being $D_0 = 2.9 \times 10^{-7}$ m^2/s. The number of solute sites per W atom is considered to be $\beta = 1$ and the lattice constant for W is $a_0 = \sqrt[-3]{\rho_W}$, where ρ_W is W atom density.

TESSIM code in such form, as presented by Eqs. (1), was used for the simulation of TDS spectra, where temperature is linearly increased with time and deuterium flux out of the sample is followed. In this case the Dirichlet boundary condition with constant deuterium concentration set to 0 was assumed on the surface of tungsten as usually taken in the literature.

In order to describe low energy hydrogen atom interaction with W, equations describing processes on the surface had to be coupled with the TESSIM code. These equations are written in terms of fluxes of particles on and off the surface. On the vacuum side of the surface we consider the flux of adsorbing atoms Γ^{ads} and the flux of desorbing molecules produced by Eley-Rideal and Langmuir-Hinshelwood recombination processes [18], Γ^{ER} and Γ^{LH}, respectively. We also take into account the flux of atoms migrating from the surface to the bulk, Γ^{bulk}, and from the bulk to the surface, Γ^{surf}. According to [19, 20] the fluxes are expressed as:

$$\begin{aligned}
\Gamma_j^{ads} &= \frac{\Gamma_0}{\eta^{surf}} (1 - R) \left(\eta_j^{surf} - c_{Aj}(t) \right), \\
\Gamma_j^{ER} &= \Gamma_0 \sigma_{ER} \, \delta_W \, c_{Aj}(t), \\
\Gamma_j^{LH} &= 2 k_{LH} \, (\delta_W \, c_{Aj}(t))^2 \, \mathrm{e}^{-2E_j^{ch}/k_B T}, \\
\Gamma_j^{bulk} &= \nu_j \, \delta_W \, c_{Aj}(t) \, \mathrm{e}^{-(E_j^{ch} + E^{bulk})/k_B T}, \\
\Gamma_j^{surf} &= \frac{D(T(t))}{a_0^2 \, \eta^{surf}} \, \delta_W \, c^{sol}(0,t) \left(\eta_j^{surf} - c_{Aj}(t) \right).
\end{aligned} \tag{2}$$

Different adsorption site types can exist due to various possible relative positions of the adsorbed atom on the crystal lattice surface, therefore index $j = 1, \ldots, N_{ads}$ denotes different adsorption site types. The dimensionless concentration of j-th adsorption site type is η_j^{surf} with $\eta^{surf} = \sum_j \eta_j^{surf}$ and the dimensionless areal concentration of hydrogen atoms is $c_{Aj}(t)$. Both dimensionless quantities are obtained by normalization to the areal density of W atoms δ_W. The concentration of solute hydrogen in the sub-surface, at the position $x = 0$, is $c^{sol}(0,t)$ and the flux of deuterium atoms to the surface is Γ_0. The reflection coefficient of W surface was theoretically determined for these low energy D atoms to be $R = 0.85$ [15], which is in agreement within the uncertainty with experimental results, reported in [11]. The rate of desorbing molecules is determined by the cross-section for Eley-Rideal recombination $\sigma_{ER} = 10^{-21}$ m^2 [11, 21] and by the desorption rate constant for Langmuir-Hinshelwood recombination $k_{LH} = a_0^2 \nu_j$, which was taken from [22] to be 0.07 cm^2/s. All

energies are denoted in Fig. 1, where potential curves for hydrogen atom and hydrogen molecule interaction with a metal as a function of the distance from the surface are shown.

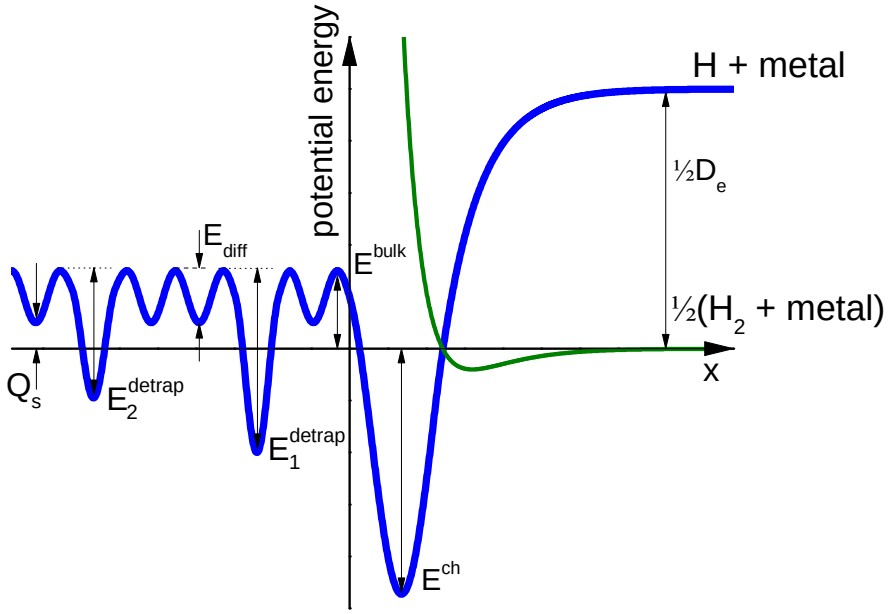

Figure 1: The potential energy for hydrogen atom (blue line) and hydrogen molecule (green line) on a metal as a function of the distance from the surface x.

Hydrogen surface areal concentrations for all adsorption site types are calculated by solving N_{ads} independent flux conservation equations

$$\delta_W \frac{dc_{Aj}}{dt} = \Gamma_j^{ads} - \Gamma_j^{LH} - \Gamma_j^{ER} + \Gamma_j^{surf} - \Gamma_j^{bulk}. \tag{3}$$

The processes on the surface are fast with the characteristic times in the order of μs. Therefore, stationary conditions on the surface are quickly accommodated to a sudden change of the incident atom flux. Assuming that stationary conditions are present at any given moment, the equation (3) can be simplified by setting the left-hand side of the equation to zero. Subsurface concentration is coupled with the bulk diffusion by equation:

$$-D(T(t))\,\rho_W \frac{\partial c^{sol}(0,t)}{\partial x} = \sum_{j=1}^{N_{ads}} \left(\Gamma_j^{bulk} - \Gamma_j^{surf}\right), \tag{4}$$

which presents a Neumann boundary condition for the concentration of solute hydrogen, used for solving Eqs. (1).

3 EXPERIMENT

This experiment was performed using four self-ion damaged recrystallized polycrystalline W samples. Samples were first chemo-mechanically polished to a mirror finish according to the procedure proposed by Manhard et al. [23]. After polishing the samples were heated in ultra-high vacuum to 2000 K for 2 min for recrystallization, what resulted in grain size of 10-50 μm [24]. Self-ion damaging was performed with 20 MeV W^{6+} ions at room temperature with the fluence of 7.9×10^{17} at/m^2 [25]. This resulted in 2 μm thick damaged layer with 0.5 dpa at the damage peak, as calculated by SRIM 2013 software [26] using a displacement energy $E_d = 90$ eV, lattice binding energy $E_L = 3$ eV and the "full cascade option". The calculated damage profile is included in Fig. 2.

Samples were mounted on a temperature controlled heater in the INSIBA experimental vacuum chamber. The experimental setup is described in detail in [27]. Samples were exposed to low energy (0.28 eV) deuterium atom beam with a flux density of 4.2×10^{18} D/m^{2}s at the analyzing beam position for approximately 121 hours, resulting in a fluence of 1.8×10^{24} D/m^2. Each sample was exposed at different sample temperature, namely 450 K, 500 K, 550 K and 600 K. During the exposure the deuterium depth profiles were measured *in situ* using NRA technique with ^3He ion beam, utilizing nuclear reaction $^3He(D,p)\alpha$. A ^3He ion beam of five different energies was used and the energy of the protons was analyzed. This enables us to deduce the D depth profile in the material down to about 7 μm with a resolution of 0.2-0.8 μm in the first 2 μm of the material and with a resolution of 0.8-2 μm deeper in the bulk. By measuring at different exposure times the time evolution of deuterium diffusion and retention in lattice defects in the bulk can be followed. After the exposure thermodesorption spectroscopy was performed *ex situ* in order to determine the trap concentrations and detrapping energies of deuterium atoms in bulk defects. Samples were heated with the heating rate of 15 K/min and a quadrupole mass spectrometer was used to monitor the desorbing species, including masses 2, 3 and 4. Details about the TDS setup and the calibration procedure can be found in [28].

4 RESULTS

Deuterium depth profiles were measured at certain times during the exposure and are shown in Fig. 2 for each exposure temperature. A clear temperature dependence of the deuterium diffusion range after 121 hours can be observed. For the sample temperature of 600 K the entire damaged layer is filled with deuterium, whereas for the temperature of 450 K only the first 0.5 μm are populated. Moreover, higher D concentration is found in depth of samples exposed at lower temperature, namely the maximum concentration in the sample exposed at 450 K was 0.5 at. % whereas for 600 K it was around 0.36 at. %.

Integrated deuterium amounts as a function of exposure time, obtained by summing D concentration over the NRA information depth, are shown in Fig. 3 for all exposure temperatures. The rate at which the damaged layer fills with deuterium depends strongly on the sample temperature. At 450 K the integrated D amount is approximately 20 % of the amount found at 600 K after the same exposure time of 121 hours.

The thermodesorption spectra were recorded for the four self-damaged W samples after

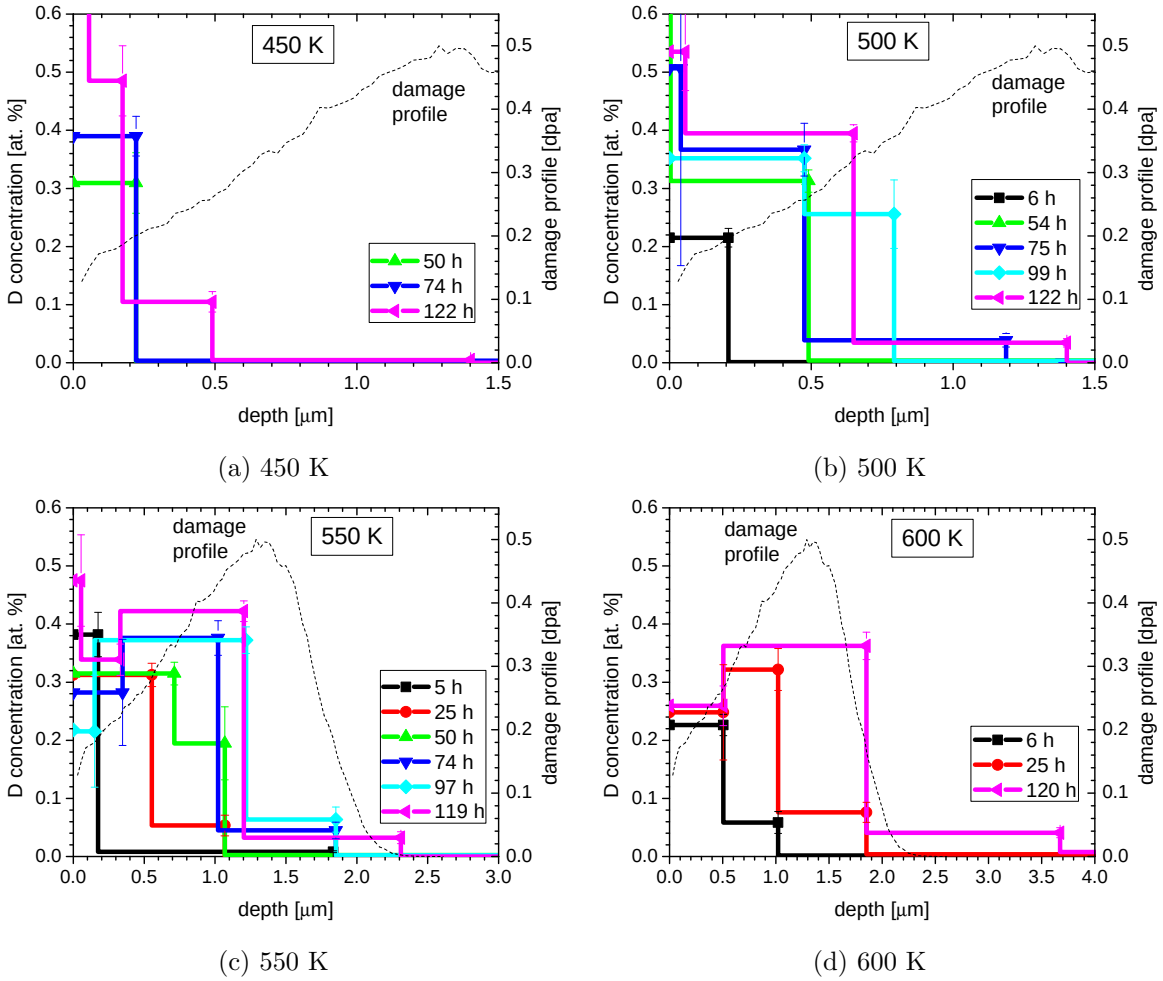

(a) 450 K

(b) 500 K

(c) 550 K

(d) 600 K

Figure 2: Deuterium concentration depth profiles at different times during D atom exposure at 450 K, 500 K, 550 K and 600 K. Damage profiles, determined by SRIM 2013, are also included.

D atom loading. Deuterium effusion fluxes, shown in Fig. 4, were determined as a sum of mass 4 (D_2) and mass 3 (HD) contributions. The observed peaks are a result of a collective effect of D diffusion, trapping, detrapping, self-clustering, etc. Only one peak is visible for the sample loaded at 600 K and is positioned at approximately 850 K. This is indicating that only one trapping site type is filled at this temperature. For the sample temperature of 550 K two peaks are visible in the spectrum, whereas for the lowest two temperatures three peaks are visible. One can also observe that the high temperature peak shifts to the right with decreasing exposure temperature. In a previous study [10] an identical sample was exposed at 500 K to a D atom beam fluence high enough to populate the entire damaged layer. There, only two peaks were observed, therefore we can assume that the additional middle peak in the current study is only due to the damaged layer being only partially filled with D atoms and not due to additional trapping site type. Namely, during the heating of a partially filled sample, atoms do not diffuse only towards the surface but also deeper into depth until a flat D concentration profile throughout the damaged layer is achieved. After

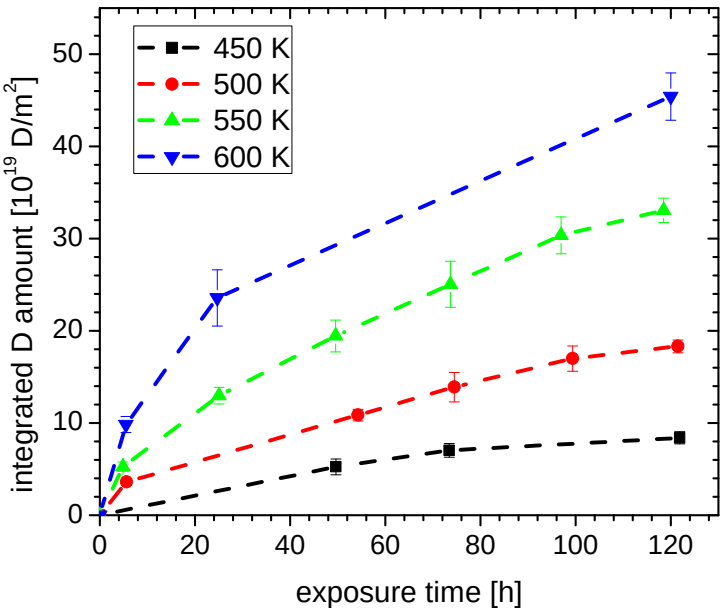

Figure 3: Time evolution of integrated deuterium amount within the NRA information depth for exposure temperatures of 450 K, 500 K, 550 K and 600 K.

that, a D flux towards the surface depletes the deuterium out of the sample. This results in a peak with additional low temperature shoulder or two separated peaks in the TDS spectrum, depending on the initial range of D atoms.

5 SIMULATION

The TESSIM code without surface processes was first used to simulate the TDS spectra. Simulation results are shown in Fig. 4 for all exposure temperatures. For the initial conditions we used D range and concentration, as determined from the D depth profiles measured by NRA. We assumed that each trap type is distributed homogeneously through the damaged layer down to a depth of 2 μm, not following the calculated displacement damage profile obtained by SRIM. This is justified by a homogeneous D depth profile obtained by NRA and homogeneous depth distribution of defects observed by scanning transmission electron microscopy [10]. Moreover, it was shown by 't Hoen et al. [29] that the damage level of a self-damaged tungsten saturates at around 0.2 dpa what in our case results in a homogeneous damage distribution throughout the most of the damaged layer. The exposure temperature of 450 K was assumed to be low enough for both traps to be saturated with D atoms. This enabled us to determine the total concentration of both traps. According to data reported in [10] D retention reduces by about 5 % due to defect annealing when the temperature is increased from 500 K to 600 K. This small change we neglected in this study. The TDS spectrum of the sample exposed at 600 K was used to determine the detrapping energy

and trap density of the high energy trap type, being 1.87 eV and 40.9×10^{19} traps/m^2, respectively. The simulation confirmed that reducing the D range results in an additional low temperature shoulder or peak positioned between the low and high temperature peak, as observed in the TDS spectra of samples, exposed at lower temperatures. The position of the lowest temperature peak was used to determine the detrapping energy of low energy trap type, being 1.6 eV. The density of the low energy trap type was determined as the difference between the integrated D amount and the D amount of the high energy trap type, which results in the trap density of 12.4×10^{19} traps/m^2. Such detrapping energies were interpreted to belong to jogged dislocation lines and dislocation loops for low and high energy trap type, respectively [13]. This set of parameters was used in the following simulations, where D uptake at different sample temperatures was simulated.

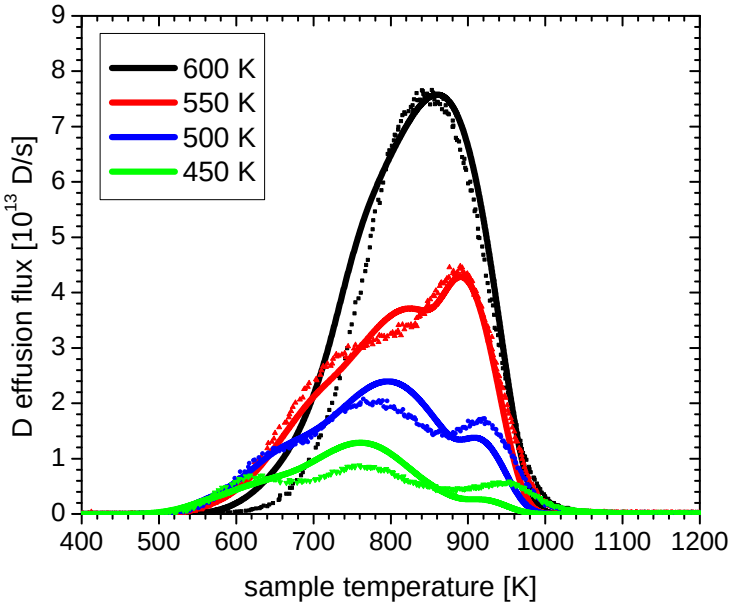

Figure 4: Simulated (solid lines) and measured (dotted lines) deuterium thermodesorption spectra for self-damaged tungsten samples, exposed to D atoms at different temperatures. Heating rate was 15 K/min.

Our next step was to determine the unknown surface parameters, i.e. adsorption energies E^{ch}, concentrations of adsorption sites η^{surf} and the height of the potential barrier E^{bulk}. These parameters were obtained by fitting the experimentally determined integrated D amounts in the samples with the data obtained from the TESSIM code with surface processes included. The fitting procedure was performed using the simulated annealing algorithm [30], minimizing $\chi^2 = \sum_i \frac{\left(y_i^{exp} - y_i^{model}\right)^2}{\sigma_i^2}$, where σ_i is the uncertainty of the i-th experimental point. For this modeling two adsorption site types were assumed, since experimentally [22] two adsorption site types were found on single crystal W with crystallographic orientation (100) and (110). The preferential crystallographic orientation of this specific W material is (100)

as reported by Manhard et al. [24] and confirmed by X-ray diffraction (XRD) performed by the Advanced materials department at Jožef Stefan Institute. Results obtained at different exposure temperatures were all fitted simultaneously since the values of fitting parameters should be the same for all cases. The obtained values of the fitting parameters are shown in Table 1. For the different temperatures as well as for the different fluence steps the integrated D amounts could be reproduced with high accuracy, as shown in Fig. 5.

Table 1: The values of the fitting parameters, obtained by fitting integrated deuterium amounts in the samples.

E_1^{ch} [eV]	η_1^{surf} [10^{19} D/m^2]	E_2^{ch} [eV]	η_2^{surf} [10^{19} D/m^2]	E^{bulk} [eV]
0.68 ± 0.02	0.51 ± 0.05	0.71 ± 0.02	1.1 ± 0.1	0.733 ± 0.003

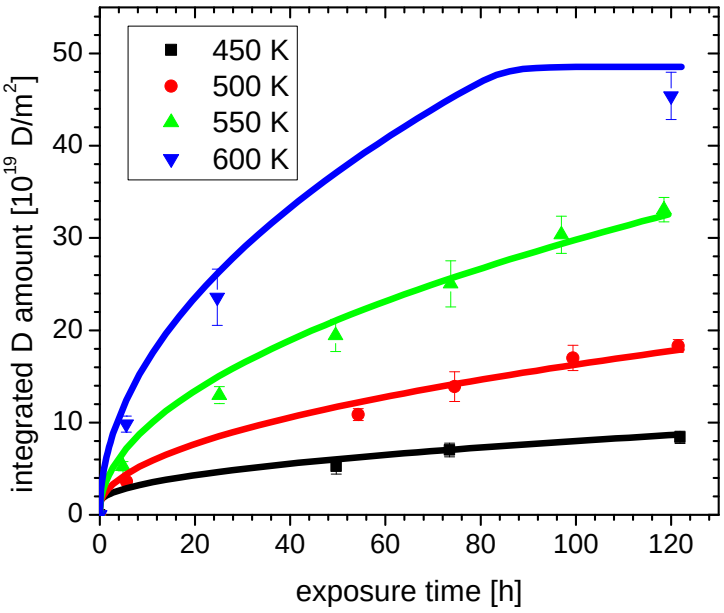

Figure 5: Time evolution of measured (dots) and modeled (lines) integrated deuterium amounts within the NRA information depth for exposure temperatures of 450 K, 500 K, 550 K and 600 K.

We have also compared the simulated deuterium depth profiles to the experimentally obtained ones. We found a good agreement between the simulation and experimental data, as shown in Fig. 6. The calculated diffusion range coincides nicely with the diffusion range, determined by the NRA technique.

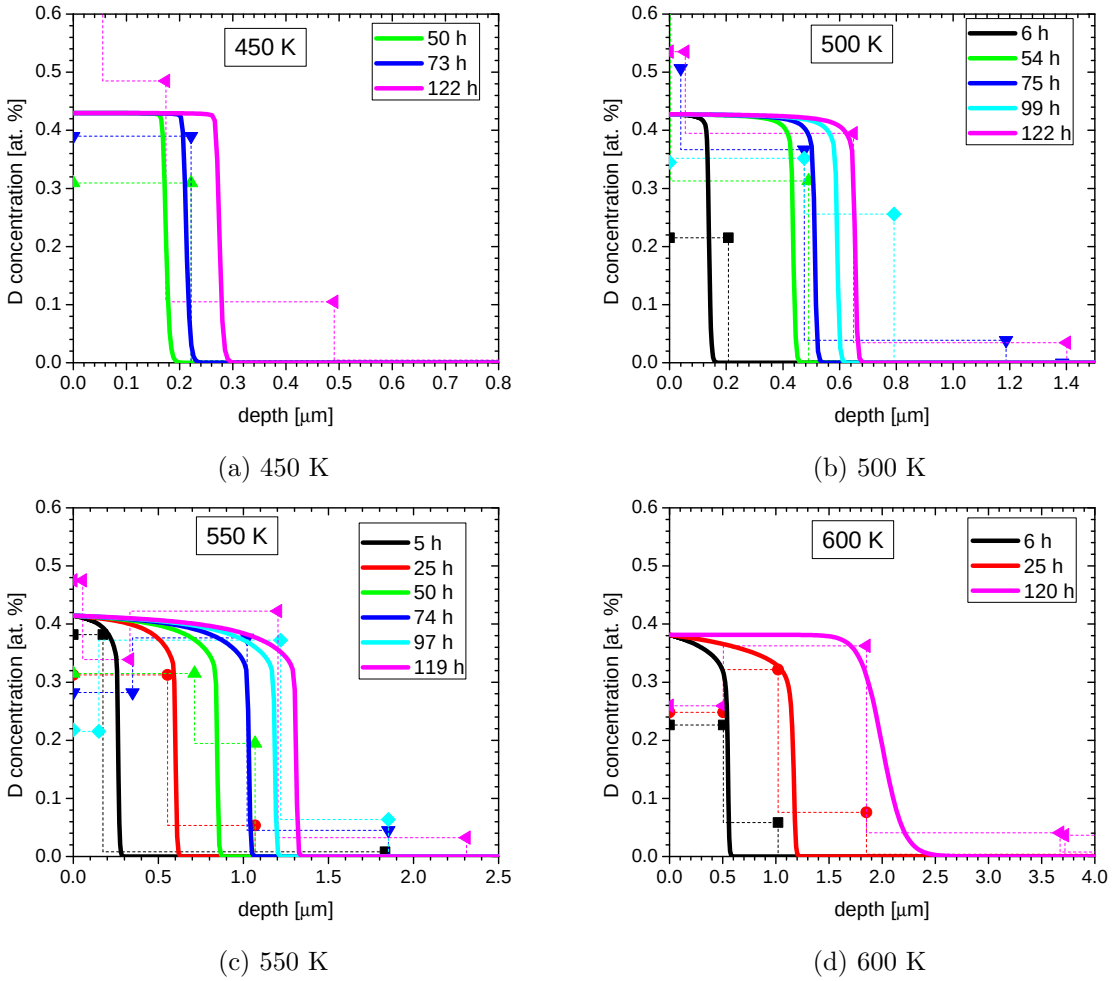

(a) 450 K

(b) 500 K

(c) 550 K

(d) 600 K

Figure 6: Simulated (lines) and measured (dots) deuterium concentration depth profiles at different times during D atom exposure at 450 K, 500 K, 550 K and 600 K.

6 COMPARISON TO PLASMA LOADING

When comparing D retention for W samples prepared in the same manner and exposed to D atoms [10] or low energy (15 ev/D) D plasma [9, 25] for sample temperatures of around 400 - 500 K the retention is of about a factor of three higher in the case of plasma exposure. In order to explain this difference in D atom to D plasma loading, we have modeled the results presented by Markina et al. [9]. There, the same polycrystalline W sample was recrystallized and self-damaged to a damage level of 0.9 dpa in the damage peak. Then it was exposed at 400 K to D plasma with flux density of 5×10^{19} D/m^{2}s for 48 hours. Depth profile and TDS spectrum were recorded after D plasma exposure, obtaining a homogeneous depth profile with 1.5 at. % of D in the damaged layer and two desorption peaks, as shown in Fig. 7. We have modeled the experimental results to determine the trapping energies and the trap densities and to compare these values to those obtained by simulating D atom loading. Experimental TDS spectrum and the corresponding simulation result are shown in Fig. 7.

Again, two different trap types were used to model D plasma loading. The detrapping energy for high energy trap type was determined to be 1.69 eV with trap density of 100.4 $\times$

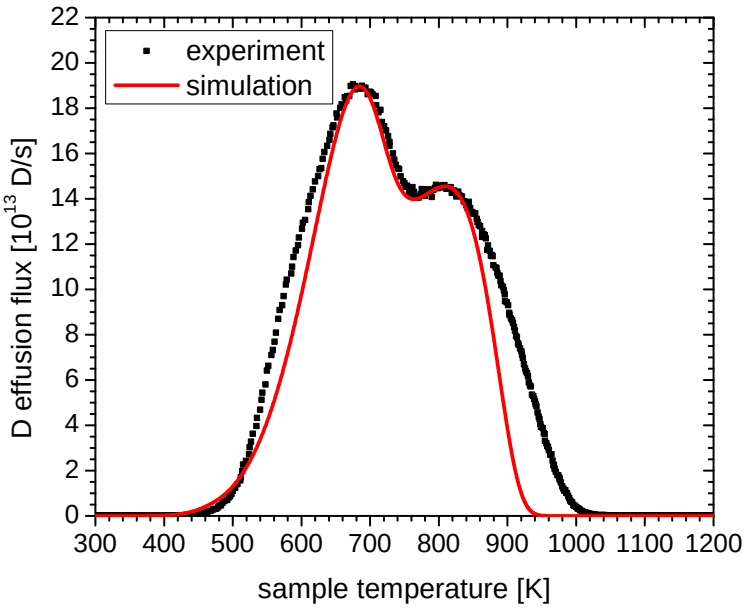

Figure 7: Deuterium thermodesorption spectra for self-damaged tungsten samples, exposed at 400 K to D plasma from [9]. Simulated spectrum is also included as a solid line.

10^{19} traps/m^2. For the low energy trap type the detrapping energy is 1.36 eV and the trap density is 86.8×10^{19} traps/m^2. Both detrapping energies are about 0.2 eV lower compared to energies obtained for D atom loading. Moreover, trap densities are drastically increased in the case of D plasma loading. We applied the TESSIM code for D atom loading with included surface processes, assuming that such concentration of traps is available also for atom loading and taking the same values for trap energies as obtained for plasma loading. We obtain higher D concentrations for all exposure temperatures, mainly on the account of the high energy trap type. Low energy trap type is significantly occupied only at the lowest two exposure temperatures. At 450 K the higher energy trap type is saturated, whereas the occupation of the low energy trap type is 50 %. This gives the D concentration of 1.16 at. %. At the highest exposure temperature of 600 K the occupations of high and low energy trap type are 86.5 % and 1.1 %, respectively, resulting in D concentration of 0.71 at. %. A possible explanation for the trap density increase obtained for plasma loading could be the creation of additional traps during plasma loading. The low D ion energy of around 15 eV is too low to create any displacement damage, however additional defects could be formed due to direct implantation of D ions. The presence of D in the lattice could induce stress which reduces a defect formation energy [31]. Moreover, thermodynamical calculations show a formation of hydrogen-vacancy clusters for hydrogen concentrations above a critical value [32]. Another possible explanation is that a different modeling approach is needed in order to be able to describe both plasma and atom loading with the same set of parameters. Namely, density functional theory (DFT) was used to show the ability of the lattice defects, such as vacancies [33] and dislocations [34], to store more than one hydrogen atom. The detrapping energy is then fill level dependent, i.e. the energy slowly decreases for higher number of hydrogen

atoms trapped in a single trap. This would explain our shift of detrapping energies to lower values for D plasma loading. A TDS peak, corresponding to individual trap type, consists of multiple peaks corresponding to different fill level of the trap. Since plasma loading was performed with much higher D flux density and direct implantation of ions in the bulk of the material is possible, the stationary condition is achieved at higher fill level of traps compared to low flux density D atom loading. Higher fill level results in the shift of the TDS peaks to lower temperatures and also manifests as higher trap density in models considering only one D atom per trap.

7 DISCUSSION AND CONCLUSIONS

Deuterium atom loading in self-damaged W samples at different sample temperatures was studied experimentally by NRA and TDS. Using the TESSIM code including the processes on the surface and transition of atoms to the bulk and back to the surface enabled us to model the obtained experimental results.

First, we have compared the determined adsorption energies with the values reported by Tamm and Schmidt [22]. Two desorption site types, β_1 and β_2, were observed on a single crystal W with crystallographic orientations of (100) and (110). These crystallographic orientations are also present on our polycrystalline samples as determined by XRD analysis. For the orientation of (100) the reported desorption energies are (1.13 ± 0.04) eV and (1.39 ± 0.04) eV for β_1 and β_2 site type, respectively. For the (110) orientation the corresponding desorption energies are (1.16 ± 0.04) eV and (1.41 ± 0.04) eV. Since the desorption energy is twice the adsorption energy, $E_i^{des} = 2E_i^{ch}$, our values for desorption energies are (1.36 ± 0.04) eV and (1.42 ± 0.04) eV. These values are in good agreement with the β_2 desorption site type on both, (100) and (110) crystallographic orientations. However, one should notice that our determined values for adsorption energies are almost the same within their uncertainties. Therefore we have performed additional simulation with only one adsorption site type. The chosen adsorption energy was the mean of previous two values $E^{ch} = 0.7$ eV and the density of adsorption sites was the sum of previous values $\eta^{surf} = 1.61 \times 10^{19}$ D/m^2. This additional simulation resulted in a similarly good fit compared to the previous simulation with two adsorption site types.

From the simulation of the experimental results the determined potential barrier is $E_{bulk} = (0.733 \pm 0.003)$ eV, giving the activation energy for migration from the surface to the bulk of (1.41 ± 0.02) eV and (1.44 ± 0.02) eV for the two adsorption site types. The determined activation energies are similar to those obtained by Hodille et al. [13], (1.33 ± 0.04) eV and (1.55 ± 0.02) eV. There, experimental results from [10] and [11] were modeled by MHIMS code [35] with included surface processes. Diffusion parameters obtained by DFT calculations were used ($E_{diff} = 0.2$ eV), whereas experimentally obtained values from [17] ($E_{diff} = 0.39$ eV) were used in our present study. Since deuterium atom absorption in W is a surface limited process, similar modeling parameters values were determined in both studies, even though different diffusion parameters were used.

According to Fig. 1, the heat of solution is defined as $Q_s = E_{bulk} - E_{diff}$. Taking into account the diffusion barrier for tungsten $E_{diff} = 0.39$ eV [17] and the value for E_{bulk} as determined in this study, the calculated heat of solution is $Q_s = (0.343 \pm 0.003)$ eV. This

value is approximately three times lower compared to the value, reported by Frauenfelder [17], $Q_s = 1.04$ eV. To match this value for the heat of solution, the potential barrier for migration into the bulk should be $E_{bulk} = 1.43$ eV. However, the simulation showed that this value is too high to describe our experimental data since the migration from the surface to the bulk is then too slow and integrated D amount is far too low. Therefore, in this additional simulation with the fixed, higher value for the potential barrier E_{bulk} we also allowed direct penetration to the bulk of the material for some fraction of impinging deuterium atoms. This is motivated by molecular dynamics (MD) simulation that showed some fraction of D atoms with energies below 1 eV could penetrate to the subsurface. This fraction can be 0 or 0.05, depending on the chosen interaction potential between tungsten and D atom [36]. However, we needed to use much larger fractions of penetrating atoms than predicted by the MD simulation in order to compensate for the negligible migration from the surface to the bulk of the material due to high potential barrier. The penetration depth was taken to be 0.2 nm [15] and the implantation distribution was assumed to be a Gaussian function with the center of the peak at the penetration depth and standard deviation of 0.1 nm.

Figure 8 is showing the integrated D amounts after the exposure to D atoms for 121 hours as a function of exposure temperature. Experimental results and simulation with $E_{bulk} = 0.733$ eV and no direct atom implantation are compared to modeling results, where $E_{bulk} = 1.43$ eV was used and 20 % and 80 % of unreflected impinging D atoms were allowed to penetrate directly into the bulk. We found a huge discrepancy between the temperature dependence of experimental results and modeling with high value of E_{bulk}. Experimental data show an increase of integrated D amount with exposure temperature, whereas modeling results have a decreasing trend. This dependence is a consequence of high value of E_{bulk}, which makes the migration into the bulk negligible. Therefore, the surface and bulk processes are decoupled and the only source of D atoms in the bulk is direct atom implantation, which is temperature independent. Since the probability for atom detrapping and desorption is higher for higher temperature, the integrated D amount is lower at higher temperature. In order to successfully model the experimental data a temperature dependent source of atoms in the bulk is needed, producing more atoms for higher temperature. This is achieved by lowering the bulk barrier E_{bulk} or by assuming temperature dependence of some other parameters (e.g. surface atom reflection).

A possible explanation for E_{bulk} being lower as compared to Frauenfelder could be the use of different W grades. In our case we used polycrystalline W samples with the grain size of 10-50 μm. Since the probing ^3He ion beam has a diameter of approximately 2 mm, we are measuring deuterium concentration over many grains and grain boundaries. Deuterium diffusion in the grain boundary can be largely enhanced compared to the diffusion through the grain itself [37]. Therefore, our determined value for the potential barrier E_{bulk} is actually an effective value, averaged over many grains and grain boundaries. However, there is no information about the grain size of the sample used in [17], therefore no direct comparison can be made.

Models, assuming only a single hydrogen atom occupying one lattice defect, are considered to be adequate for explaining simple hydrogen loading in the material. However, such models fail to describe some more complex experiments, such as e.g. low temperature isotope exchange [38]. Indeed, our simple model was capable of describing experimental results of both, D atom and plasma loading, but the values of modeling parameters differ for both

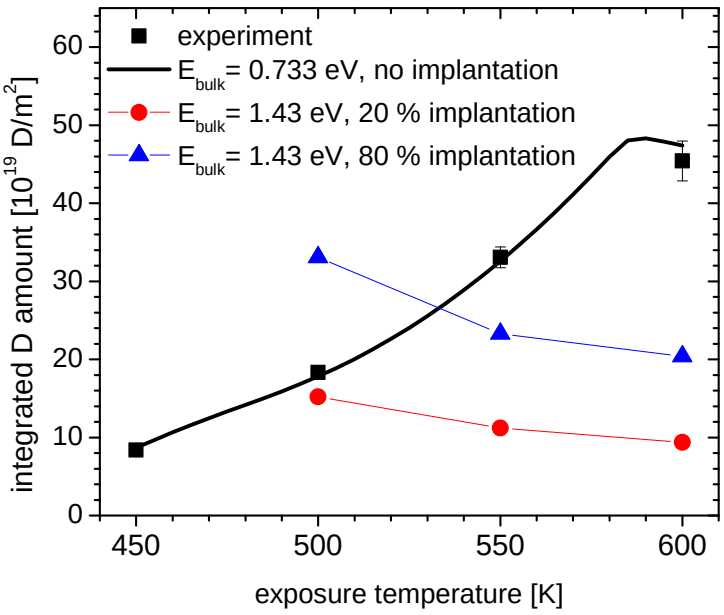

Figure 8: Integrated D amounts as a function of exposure temperature obtained experimentally (black squares) and by modeling with E_{bulk} = 0.733 eV and no direct atom implantation (black line), E_{bulk} = 1.43 eV and 20 % direct atom implantation (red circles) and E_{bulk} = 1.43 eV and 80 % direct atom implantation (blue triangles). Integrated amounts correspond to D atom exposure with a flux density of 4.2×10^{18} D/m^{2}s for 121 hours.

types of loading. This could indicate that such model is not providing a realistic picture of deuterium tungsten interaction and only effective parameter values are determined for each individual experiment. The difference in the parameter values could imply that fill level dependent model is needed also for the simulation of simple hydrogen loading experiments in order to obtain proper understanding of the studied interactions and to develop realistic models applicable for a broad range of experimental conditions, especially large flux ranges. However, at present we cannot exclude creation of additional damage due to ion implantation as a reason for the difference between atom and plasma loading.

ACKNOWLEDGMENT

This work has been carried out within the framework of the EUROfusion Consortium and has received funding from the Euratom research and training programme 2014-2018 under grant agreement No 633053. This work was done within the EUROfusion work project PFC. The views and opinions expressed herein do not necessarily reflect those of the European Commission. This work was part of the IAEA coordinated research project CRP F43021.

The authors would also like to thank Dr. Srečo D. Škapin from the Advanced materials department at Jožef Stefan Institute for performing XRD analysis of the sample.

References

[1] V. Philipps *J. Nucl. Mater.*, vol. 415, p. S2, 2011.

[2] S. Brezinsek and JET-EFDA contributors *J. Nucl. Mater.*, vol. 463, p. 11, 2015.

[3] A. S. Kukushkin, H. D. Pacher, V. Kotov, D. Reiter, D. Coster, and G. W. Pacher *Nucl. Fusion*, vol. 45, p. 608, 2005.

[4] J. Roth, E. Tsitrone, Th. Loarer, V. Philipps, S. Brezinsek, A. Loarte, G. F. Counsell, R. P. Doerner, K. Schmid, O. V. Ogorodnikova, and R. A. Causey *Plasma. Phys. Control. Fusion*, vol. 50, p. 103001, 2008.

[5] O. V. Ogorodnikova and V. Gann *J. Nucl. Mater.*, vol. 460, p. 60, 2015.

[6] Y. Hatano, M. Shimada, T. Otsuka, Y. Oya, V. Kh. Alimov, M. Hara, J. Shi, M. Kobayashi, T. Oda, G. Cao, K. Okuno, T. Tanaka, K. Sugiyama, J. Roth, B. Tyburska-Püschel, J. Dorner, N. Yoshida, N. Futagami, H. Watanabe, M. Hatakeyama, H. Kurishita, M. Sokolov, and Y. Katoh *Nucl. Fusion*, vol. 53, p. 073006, 2013.

[7] O. V. Ogorodnikova and K. Sugiyama *J. Nucl. Matter.*, vol. 442, p. 518, 2013.

[8] O. V. Ogorodnikova, Yu. Gasparyan, V. Efimov, Ł. Ciupiński, and J. Grzonka *J. Nucl. Matter.*, vol. 451, p. 379, 2014.

[9] E. Markina, M. Mayer, A. Manhard, and T. Schwarz-Selinger *J. Nucl. Matter.*, vol. 463, p. 329, 2015.

[10] A. Založnik, S. Markelj, T. Schwarz-Selinger, Ł. Ciupiński, J. Grzonka, P. Vavpetič, and P. Pelicon *Phys. Scr.*, vol. T167, p. 014031, 2016.

[11] S. Markelj, A. Založnik, T. Schwarz-Selinger, O. V. Ogorodnikova, P. Vavpetič, P. Pelicon, and I. Čadež *J. Nucl. Mater.*, vol. 469, p. 133, 2016.

[12] K. Schmid, V. Rieger, and A. Manhard *J. Nucl. Mater.*, vol. 426, p. 247, 2012.

[13] E. A. Hodille, A. Založnik, S. Markelj, T. Schwarz-Selinger, C. S. Becquart, R. Bisson, and C. Grisolia *Nucl. Fusion*, vol. 57, p. 056002, 2016.

[14] J. Roth, E. Tsitrone, A. Loarte, Th. Loarer, G. Counsell, R. Neu, V. Philipps, S. Brezinsek, M. Lehnen, P. Coad, Ch. Grisolia, K. Schmid, K. Krieger, A. Kallenbach, B. Lipschultz, R. Doerner, R. Causey, V. Alimov, W. Shu, O. V. Ogorodnikova, A. Kirschner, G. Federici, A. Kukushkin, EFDA PWI Task Force, ITER PWI Team, Fusion for Energy, and ITPA SOL/DIV *J. Nucl. Mater*, vol. 390-391, p. 1, 2009.

[15] O. V. Ogorodnikova, S. Markelj, and U. von Toussaint *J. Appl. Phys.*, vol. 119, p. 054901, 2016.

[16] K. Heinola and T. Ahlgren *J. Appl. Phys.*, vol. 107, p. 113531, 2010.

[17] R. Frauenfelder *J. Vac. Sci. Technol.*, vol. 6, p. 388, 1969.

[18] C. T. Rettner and M. N. R. Ashfold, eds., *Dynamics of Gas-Surface Interactions*. Cambridge: The Royal Society of Chemistry, 1991.

[19] M. A. Pick and K. Sonnenberg *J. Nucl. Mater.*, vol. 131, p. 208, 1985.

[20] O. V. Ogorodnikova *J. Nucl. Mater.*, vol. 277, p. 130, 2000.

[21] O. Galparsoro, R. Pétuya, J. I. Juaristi, C. Crespos, M. Alducin, and P. Larrégaray *J. Chem. Phys.*, vol. 119, p. 15434, 2015.

[22] P. W. Tamm and L. D. Schmidt *J. Chem. Phys.*, vol. 54, p. 4775, 1971.

[23] A. Manhard, G. Matern, and M. Balden *Prakt. Metalogr.-PR. M.*, vol. 50, p. 5, 2013.

[24] A. Manhard, M. Balden, and S. Elgeti *Prakt. Metalogr.-PR. M.*, vol. 52, p. 437, 2015.

[25] T. Schwarz-Selinger *submitted to Nucl. Mater. Energy*, 2016.

[26] http://www.srim.org/.

[27] S. Markelj, O. V. Ogorodnikova, P. Pelicon, T. Schwarz-Selinger, P. Vavpetič, and I. Čadež *Phys. Scr.*, vol. T159, p. 014047, 2014.

[28] P. Wang, W. Jacob, L. Gao, T. Dürbeck, and T. Schwarz-Selinger *Nucl. Instrum. Meth. B*, vol. 300, p. 54, 2013.

[29] M. H. J. 't Hoen, B. Tyburska-Püschel, K. Ertl, M. Mayer, J. Rapp, A. W. Kleyn, and P. A. Zeijlmans van Emmichoven *Nucl. Fusion*, vol. 52, p. 023008, 2012.

[30] S. Kirkpatrick, C. D. Gelatt Jr., and M. P. Vecchi *Science*, vol. 220, p. 671, 1983.

[31] L. Gao, W. Jacob, U. von Toussaint, A. Manhard, M. Balden, K. Schmid, and T. Schwarz-Selinger *Nucl. Fusion*, vol. 57, p. 016026, 2017.

[32] L. Sun, S. Jin, H.-B. Zhou, Y. Zhang, W. Zhang, Y. Ueda, H. T. Lee, and G.-H. Lu *J. Phys.: Condens. Matter*, vol. 26, p. 395402, 2014.

[33] N. Fernandez, Y. Ferro, and D. Kato *Acta Mater.*, vol. 94, p. 307, 2015.

[34] D. Terentyev, V. Dubinko, A. Bakaev, Y. Zayachuk, W. Van Renterghem, and P. Grigorev *Nucl. Fusion*, vol. 54, p. 042004, 2014.

[35] E. A. Hodille, X. Bonnin, R. Bisson, T. Angot, C. S. Becquart, J. M. Layet, and C. Grisolia *J. Nucl. Mater.*, vol. 467, p. 424, 2015.

[36] P. N. Maya *J. Nucl. Matter.*, vol. 480, p. 411, 2016.

[37] U. von Toussaint, S. Gori, A. Manhard, T. Höschen, and C. Höschen *Phys. Scr.*, vol. T145, p. 014036, 2011.

[38] K. Schmid, U. von Toussaint, and T. Schwarz-Selinger *J. Appl. Phys.*, vol. 116, p. 134901, 2014.